Supporting Information for:

Enhancing NIR-to-visible Upconversion in a Rigidly Coupled Tetracene Dimer: Approaching Statistical Limits for Triplet-Triplet Annihilation using Intramolecular Multiexciton States

Alexander T. Gilligan, Raythe Owens, Ethan G. Miller, Nicholas F. Pompetti, and Niels H. Damrauer

Table of Contents

S1. Experimental Setup

S1.1. Sample Preparation

S1.1.1. Non-Upconversion Samples (UV-Vis, TCSPC, Steady-State Emission, Nanosecond Transient Absorption)

Samples of interest were dissolved in spectroscopic grade toluene (from Alfa Aesir) within a 1 cm UV-Quartz cuvette with a Kontes valve top. They were then deaerated via sparging with Ar gas for ~30 minutes. Samples were monitored for degradation via UV-Vis absorption spectroscopy after experiments. Absorption measurements of samples in chloroform were performed using spectroscopic grade solvent from Sigma-Aldrich without sparging.

S1.1.2. Upconversion Samples (UV-Vis, Steady-State Emission, Nanosecond Transient Absorption)

Masses of TIPS-BTX, TIPS-Tc and PdPc were weighed and dissolved in spectroscopic grade toluene (from Alfa Aesir) to form separate stock solutions. Samples were then prepared by volumetrically mixing the stock solutions and diluting with additional spectroscopic grade toluene. Samples were then transferred to a 1 cm UV-Quartz cuvette with a Kontes valve top, deaerated via sparging with Ar gas for ~45 minutes. To prevent concentration fluctuation, sparging was performed by connecting the Ar gas line to a solvent reservoir, which was then further connected into the sample cuvette. This setup allowed the samples to be sparged more vigorously and longer without observable concentration changes. Samples were monitored for signs of degradation after measurements via UV-Vis absorption spectroscopy.

S1.2. Steady-State Absorption and Emission Spectroscopy

Steady-state UV-Vis absorption measurements were performed on a HP8452A diode array UV-Vis spectrometer and Agilent Cary 5000 UV-Vis-NIR absorption spectrophotometer for

higher resolution measurements. Steady-state photoluminescence measurements were performed with an Olis SLM 8000C fluorimeter. The slit widths were set to 1 mm with a dispersion factor of 2 nm/mm, allowing for 2 nm spectral resolution. Emission spectra are dependent on the instrument setup as well as the signal from the emitting molecule. To account for this instrument-specific response, a wavelength-dependent correction factor was calculated as the multiplicative factor necessary to match the collected emission profiles of two solid emissive NIST standards (SRM 2940-B and SRM 2943) to their true profiles. This wavelength-dependent correction factor was then applied to all collected spectra to obtain the true spectra. All samples were kept at 20°C throughout the collection period via a temperature control unit coupled with a flowing water reservoir and a jacketed sample holder.

S1.3. Time-Correlated Single Photon Counting (TCSPC)

Fluorescence lifetime measurements were performed using a DeltaFlex Modular Fluorescence Lifetime System from Horiba Scientific Ltd. The sample was excited with a Horiba NanoLED-405L (405 nm, <200 ps) and emission was collected perpendicular to excitation path and with polarization set to magic angle relative to the excitation polarization to prevent anisotropic artifacts. Collected data were modeled using a single exponential decay function. Temperature was kept constant at 20°C with a Quantum Northwest TC-1 temperature control unit coupled with an aquarium pump submerged in a reservoir, and a jacketed sample holder.

S1.4. Nanosecond Transient Absorption Spectroscopy (nsTA)

Two instruments were used to collect kinetic lifetimes on nanosecond or longer timescales. The first instrument used in the collection of the nanosecond TA dynamics of TIPS-BTX shown in the main text has previously been described elsewhere.[1]

The second instrument was used for the collection of triplet lifetime of TIPS-Tc and TIPS-BTX via triplet sensitization. The pump source was an Nd:YAG (Continuum Surelite II) 10 Hz pulsed laser with 355 nm central wavelength output and ~5 ns pulse duration. The output was used either as the direct excitation source or to pump a Continuum Surelite optical parametric oscillator to obtain variable wavelength selection. The pump source was attenuated with neutral density filters to achieve pulse energies of ~150 μJ/pulse at the sample. The pump spot size was measured to have a diameter of 4 mm by FWHM. A Xenon arc lamp was used as the probe source. The probe was collimated and directed into the sample perpendicular to the excitation source, ensuring the probe's beam was well-encompassed by the pump at their overlap. Probe light after the sample was focused into a monochromator to separate probe wavelengths. Wavelength selected kinetic traces were then measured on a negatively biased PMT (Hamamatsu R928-07) and recorded with a digital oscilloscope (Picoscope 5444D).

S1.5. Steady-State Upconversion Measurements

For excitation of upconversion samples a Thorlabs HL7302M 730 nm diode controlled with a LD205C current controller and TED200C temperature monitor was used. A LTC56M collimating lens was used to collimate the diode output. Reference samples of TIPS-Tc in spectroscopic grade toluene (from Alfa Aesir) were pumped with a Thorlabs 405 nm diode. Beam power and area for fluence measurements was characterized with an Ophir Pd300-UV photodiode or an Ophir 2A-BB-9 power meter and an Ophir SF928 Beam Profile Camera. Upconverted emission was detected via the setup described in Section S1.2, and as such the same wavelength-dependent correction factor was applied to all collected spectra. Samples were temperature controlled with a VWR 1145 refrigerated constant temperature circulator set to 20°C coupled with a jacketed sample holder.

S1.6. Computational Details

Geometry optimization of TIPS-BTX was done using the basis set 6-31G(d) and functional w-97xbd and a solvent continuum model set for toluene. The TIPS groups were removed for the geometry optimization and replaced with a hydrogen atom (leaving a bare acetylene) to expedite the calculation. TD-DFT computations were set to find the transitions to the six lowest energy singlet excited states.

S2. Molar Extinction Coefficients

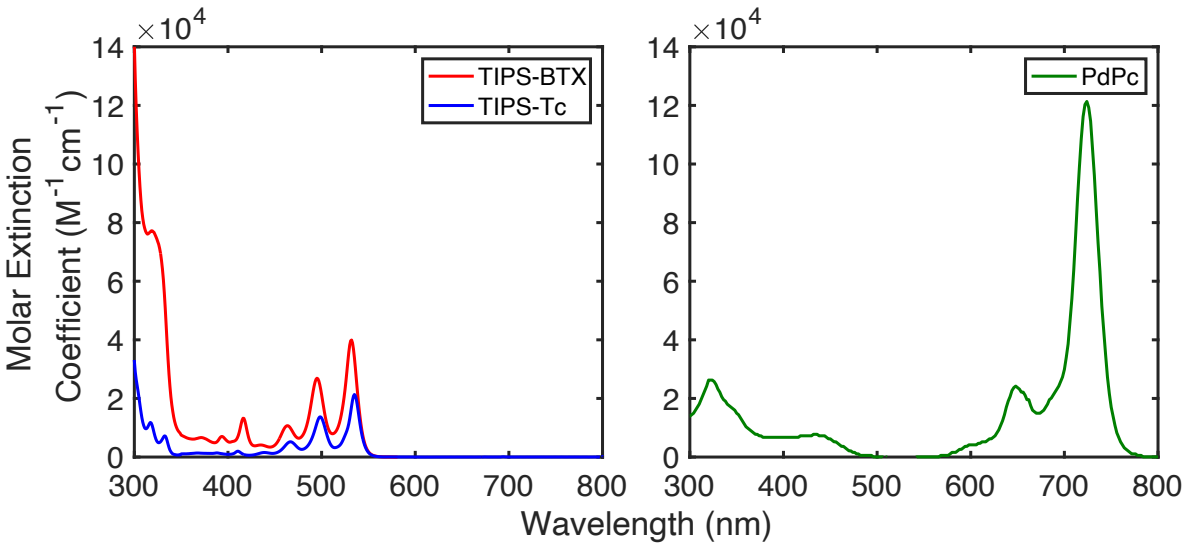

Figure S1. Molar Extinction Coefficients for TIPS-BTX/TIPS-Tc (left) and PdPc (right) in toluene. TIPS-BTX showed an approximate doubling of the molar extinction coefficient of the S_1 vibronic progression (40,000 $M^{-1}cm^{-1}$ at 0 – 0 transition) compared to TIPS-Tc (21,000 at 0 – 0 transition).

S3. Steady-State UV-Vis Absorption in Chloroform

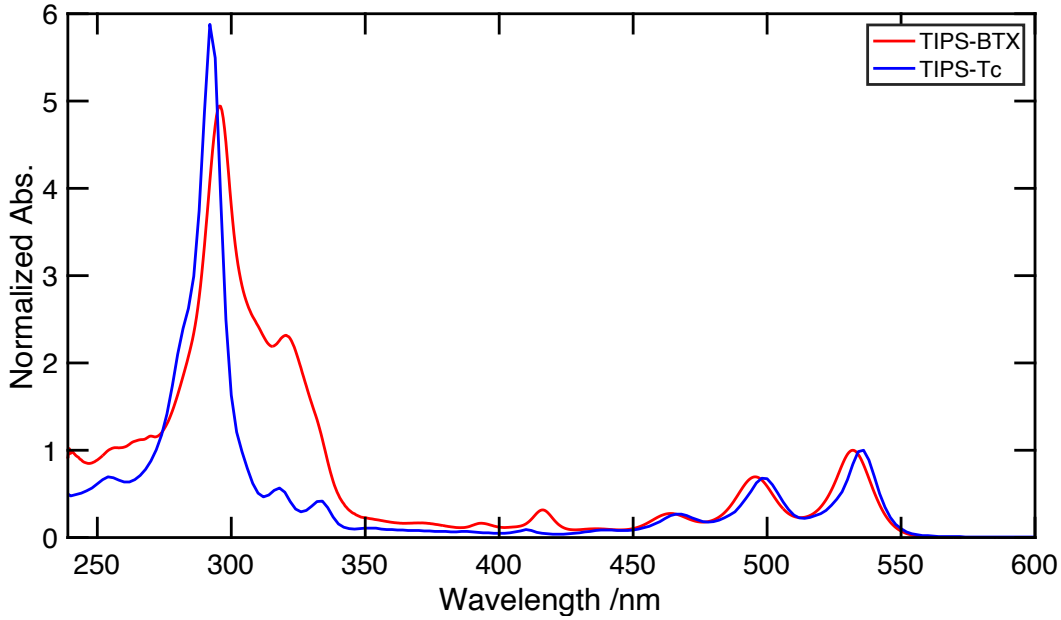

Figure S2. Normalized steady-state absorption of TIPS-BTX in room temperature chloroform to demonstrate the expected lack of Davydov-split features in the UV. The steady-state absorption of TIPS-Tc in room temperature chloroform is included for reference.

S4. UV-Vis Absorption Spectra of Upconversion Samples

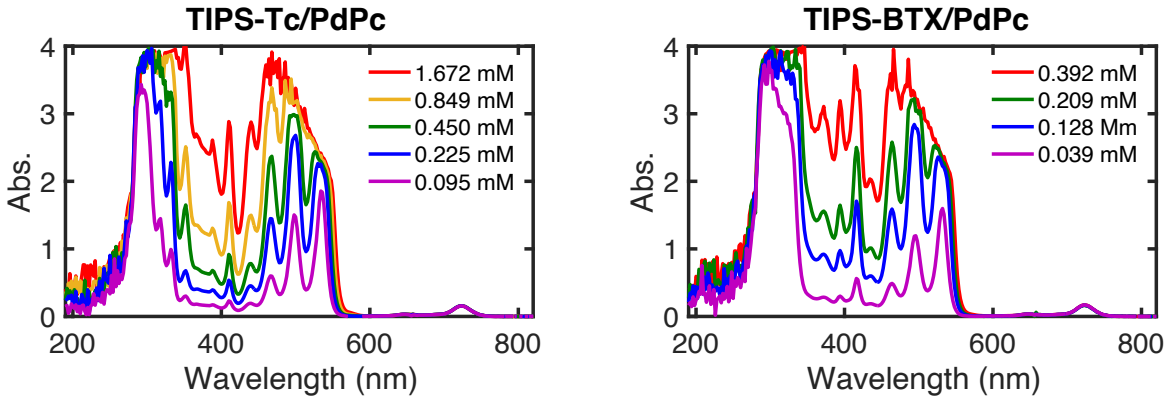

Figure S3. Steady-state absorption spectra for TIPS-Tc/PdPc (left) and TIPS-BTX/PdPc (right) upconversion samples across a range of annihilator concentrations and constant sensitizer concentration.

S5. nsTA Global Analysis of TIPS-BTX

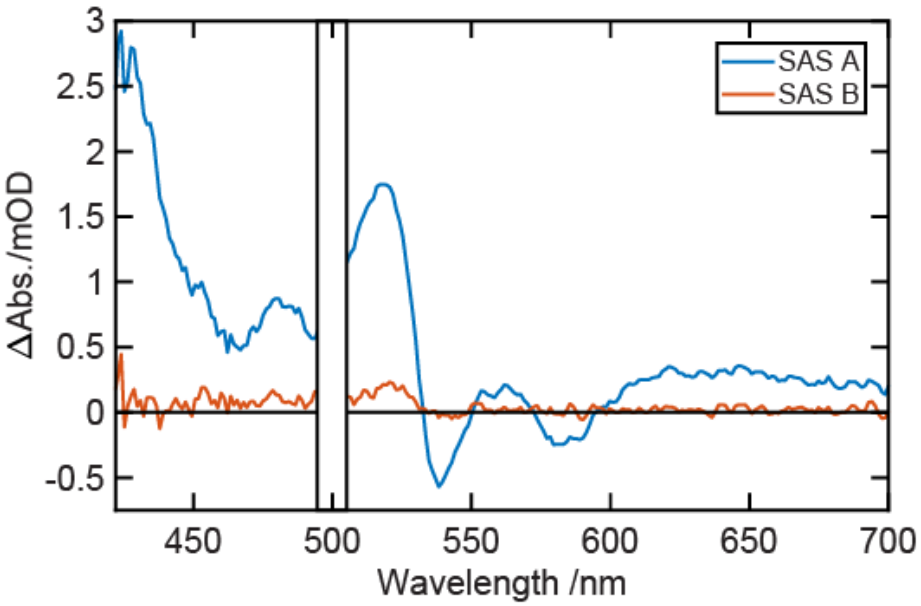

Figure S4. Two-state species associated spectra (SAS) retrieved from global analysis of nsTA collected for TIPS-BTX in room temperature toluene.

S6. Triplet Yield and TT Energy of TIPS-BTX

The triplet yield of TIPS-BTX was determined by calculating the triplet concentration at 1 μs and dividing by the initial concentration of S_1 from excitation. A time delay of 1 μs is much longer than the singlet decay lifetime (12.9 ns), but well-within the triplet decay lifetime (410 μs), such that an estimate here is expected to avoid singlet contamination while also preventing significant underestimation of the triplet yield. The triplet concentration was determined using Eq. S1, which relies on the sample path length ℓ, on data at the maximum of the triplet ESA at 520nm (i.e., ΔAbs_{T_1}), and on a determination of the change in molar extinction between the triplet and the ground state at this wavelength (i.e., $\Delta\varepsilon_{T_1}$).

$$[T_1] = \frac{\Delta Abs_{T_1}}{\Delta\varepsilon_{T_1} \times \ell} \qquad \text{S1}$$

The pathlength ℓ was taken to be the cuvette pathlength 0.2 cm. For $\Delta\varepsilon_{T_1}$ we have relied upon a previous measurement made using a norbornyl bridged TIPS-tetracene dimer called TIPS-BT1′.[1] This substitution is reasonable because the triplet is expected to be chromophore-localized in both TIPS-BT1′ and TIPS-BTX; the identical acene is directly fused to a bicyclic norbornyl substituent.

The moles of singlet excited states (mol_{S_1}) were calculated using the absorbed beam power by Eq. S2

$$mol_{S_1} = \frac{(1 - 10^{-Abs})}{N_A} \frac{E_{pump}}{E_{photon}} \quad \text{S2}$$

A sample absorbance (*Abs*) of 0.13, E_{pump} of 160 nJ and E_{photon} of 500 nm were the parameters for this experiment.

The excited singlet concentration was determined by taking moles of excited S_1 and dividing by the excitation volume using Eq. S3, with the excitation beam diameter (d = 294 μm) and cuvette length ℓ = 0.2 cm.

$$V = \pi \left(\frac{d}{2}\right)^2 \times \ell \quad \text{S3}$$

This analysis gives an upper limit for the triplet yield at ~6.5%. If this yield is attributed to singlet fission, a lower limit for the multiexciton TT yield would therefore be half the T_1 yield (a situation where 100% of the multiexciton population yielded decoupled triplets). If an equilibrium analysis (Eq. S4) is then performed to estimate the energy of the multiexciton TT state as described in an earlier work,[1] a lower limit to the equilibrium constant is calculated to be 0.0336 (3.25%/96.75%).

$$K_{eq} = \frac{^n[TT]}{[S_1]} \quad \text{S4}$$

Using the Boltzmann factor for two states (Eq. S5), at room temperature (T) this would correspond to a maximum energy (E) gap between the multiexciton TT and the S_1 of 88 meV, indicating a maximum multiexciton state energy of 2.41 eV, nearly identical to estimates for TIPS-Tc.

$$K = e^{\frac{E_{S_1} - En_{TT}}{k_B T}} \quad \text{S5}$$

In the zero-field, it is expected that the exchange interaction J is sufficiently low to result in near degeneracy of the multiexciton spin-manifold.[2]

S7. Triplet Lifetimes of PdPc and TIPS-Tc/TIPS-BTX via Triplet Sensitization

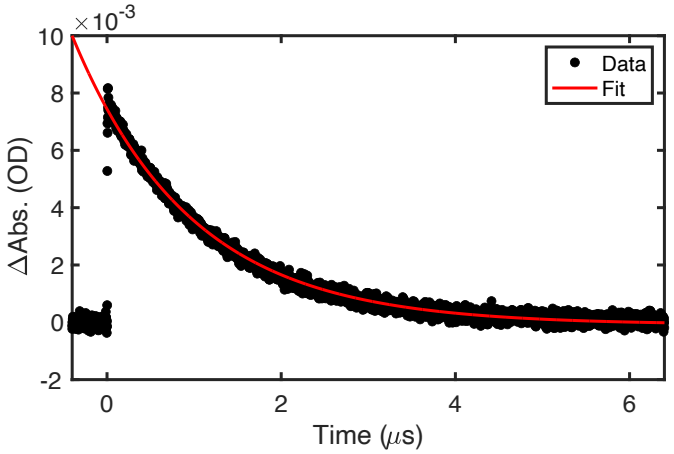

Figure S5. Kinetic trace of PdPc in toluene excited at 650 nm and observed at 600 nm. Modeled using a function with a 3.42 μs single exponential lifetime determined using least-squares fitting.

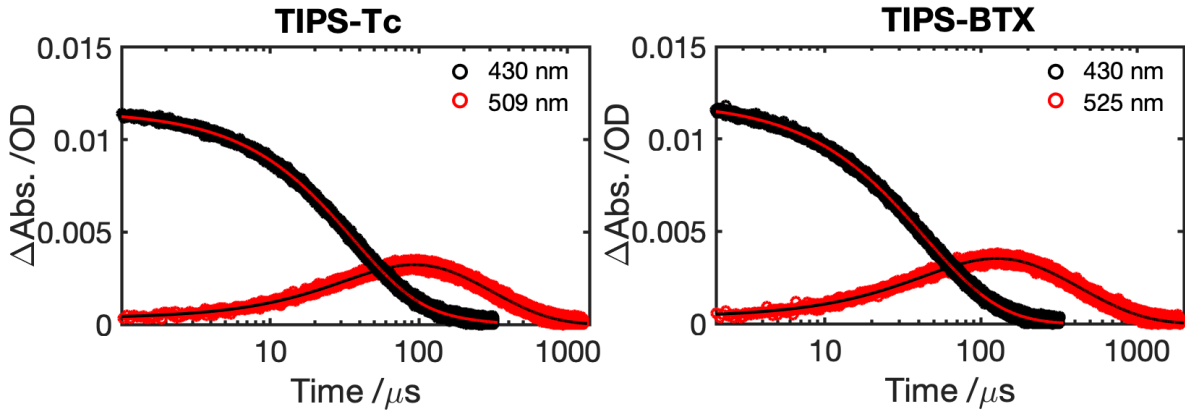

Figure S6. Kinetic traces with a bi-exponential model (solid lines) of anthracene and TIPS-Tc/TIPS-BTX in toluene. The decay of anthracene triplet (430 nm) corresponds with rise of sensitized triplet signal measured at 509 nm for TIPS-Tc and 525 nm for TIPS-BTX. For TIPS-Tc at 509 nm a bi-exponential fit returned lifetimes of 43 μs (sensitization from the anthracene triplet) and 290 μs (the TIPS-Tc triplet lifetime). For TIPS-BTX at 525 nm a bi-exponential model returned lifetimes of 57 μs (sensitization from the anthracene triplet) and 410 μs (the TIPS-BTX triplet lifetime). The absorption feature at 430 nm was fit with a single lifetime corresponding to the quenched anthracene triplet with a small (0.5 mOD) offset included due to the presence of ESA from the TIPS-Tc/TIPS-BTX triplet.

S8. Crossing Point Fluences for TIPS-Tc and TIPS-BTX

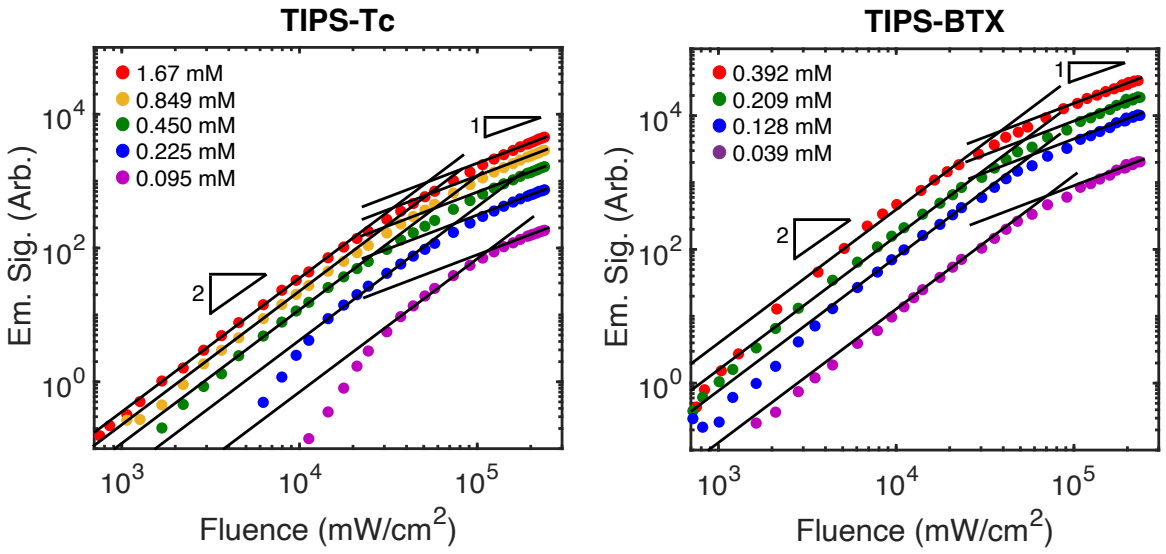

Figure S7. (left) Integrated emission intensity of five TIPS-Tc upconversion samples in toluene over experimental fluence range. (right) Integrated emission intensity of four TIPS-BTX

upconversion samples in toluene over experimental fluence range. Quadratic and linear fluence regimes shown with added lines.

The crossing point fluences demonstrated here represent the intensity threshold for which 38% of excited triplets should decay via bimolecular channels vs unimolecular triplet decay. To convert to the 50% intensity threshold often discussed, doubling the observed value here is necessary.[3] Comparison to others in the literature often yields varied intensity thresholds, even for the same system. This can be explained by the intensity threshold's dependence on many system and experimental parameters, namely the excitation wavelength, sample absorbance at the excitation wavelength, efficiency of intersystem crossing and triplet energy transfer, and the natural triplet lifetime given degree of deoxygenation. Viewed this way, it is important to note that reported intensity thresholds are not standardized, and instead must be evaluated in the context of the individual experimental conditions.

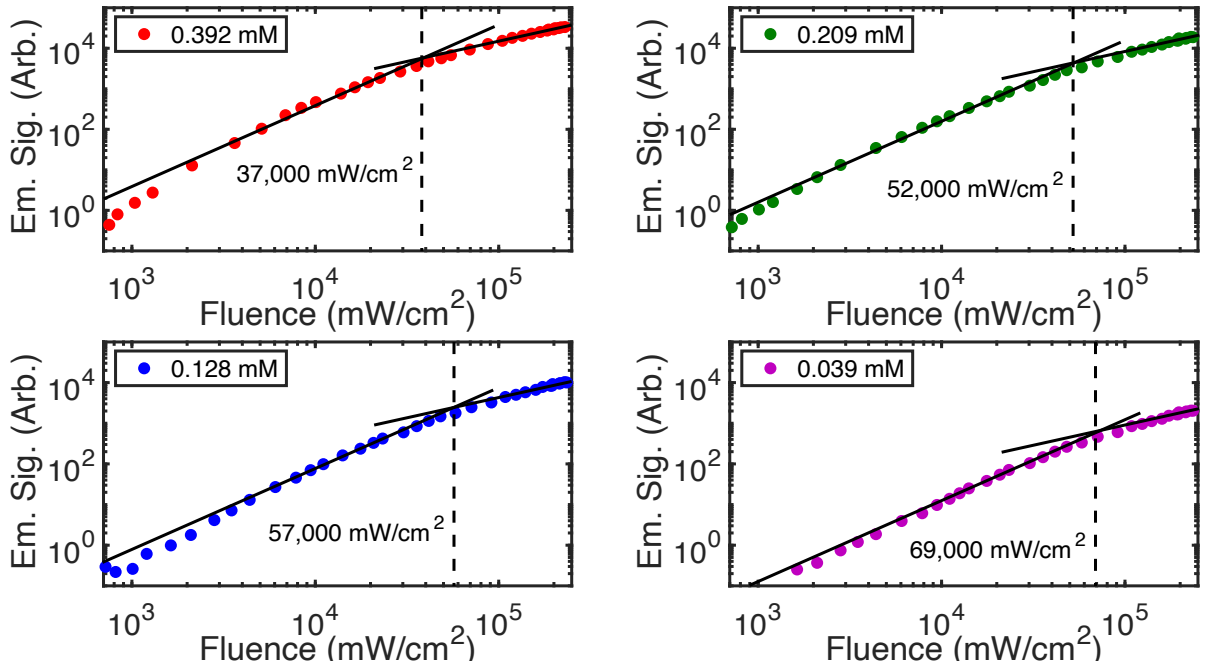

Figure S8. Integrated emission intensity of TIPS-BTX upconversion samples with observed crossing-point between quadratic/linear regimes as excitation fluence is increased.

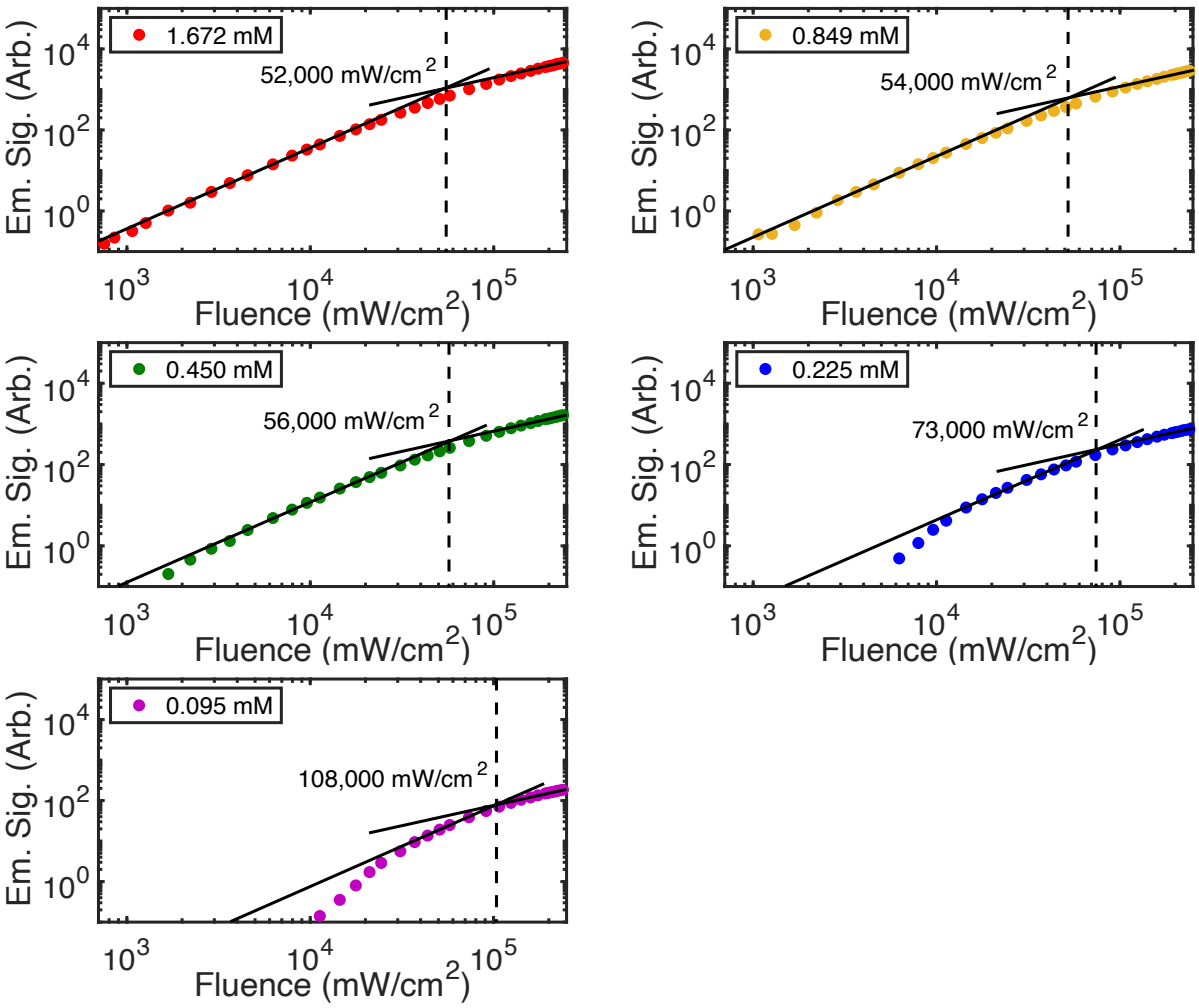

Figure S9. Integrated emission intensity of TIPS-Tc upconversion samples with observed crossing-point between quadratic/linear regimes as excitation fluence is increased.

S9. Threshold Intensity

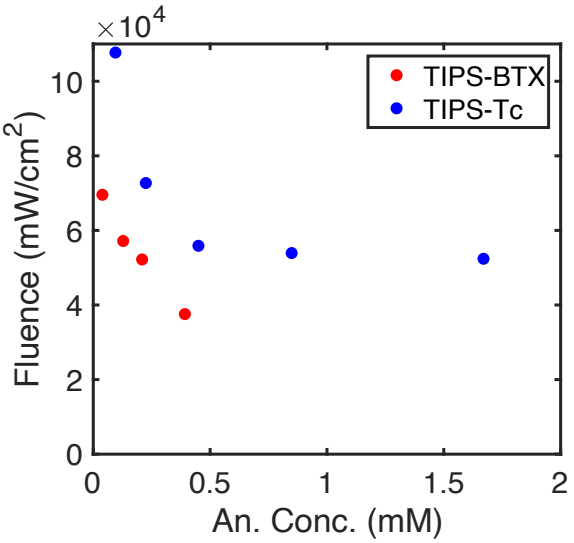

Figure S10. Observed crossing-point fluences of TIPS-Tc/TIPS-BTX upconversion samples as a function of annihilator concentration.

S10. Quantifying the Raw Upconversion Quantum Yield $\phi_{UC,raw}$

The raw upconversion quantum yield was measured relatively by utilizing deaerated, room temperature TIPS-Tc in toluene as a reference standard for the upconversion samples' emission, with a known quantum yield of 74% (ϕ_{Ref}).[4] Emission spectra were collected, corrected, and integrated (Int). The excitation source was characterized by measuring both the beam size and power to obtain the fluence, then converted into photon flux (Ex) by dividing the fluence by the energy of a photon at the excitation wavelength. The absorbance (Abs) of each sample was measured and converted to a percentage of photons absorbed by the sample via $1 - 10^{-Abs}$. The indices of refraction (η) are a characteristic of the solvent used, in this case both reference and upconversion sample were taken in toluene, with an $\eta = 1.496$. As described by Eq. S6, by accounting for the reference quantum yield, excitation fluxes, absorbance at the excitation wavelength, integrated emission intensity, and indices of refraction, the raw upconversion yield can be calculated.

$$\phi_{UC,raw} = \phi_{Ref} \times \frac{1 - 10^{-Abs_{Ref}}}{1 - 10^{-Abs_{UC}}} \times \frac{Ex_{Ref}}{Ex_{UC}} \times \frac{Int_{UC}}{Int_{Ref}} \times \frac{{\eta_{UC}}^2}{{\eta_{Ref}}^2} \quad \text{S6}$$

S11. Correction of Upconversion Emission Spectra

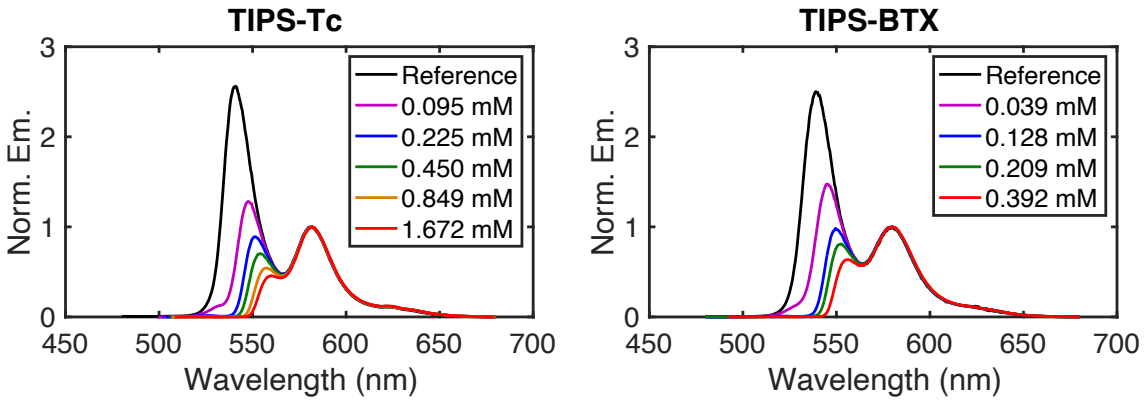

Figure S11. Full emission spectra of TIPS-Tc/TIPS-BTX upconversion samples compared to emission spectra of TIPS-Tc/TIPS-BTX reference samples. Samples containing high concentrations of annihilators undergo increasing self-absorption. Correction of the self-absorption is crucial for an accurate characterization of both upconversion efficiency and triplet-triplet annihilation efficiency.

To account for self-absorption in upconversion samples that would artificially lower the upconversion quantum yield, Eq. S7 was employed. In this expression, $\phi_{UC,raw}$ is the upconversion quantum yield measured at the final fluence point. This yield was then multiplied against the ratio of the integrated emission intensity for the upconversion sample (Int_{Sample}) and a reference sample of just the annihilator in toluene directly excited (Int_{Ref}). Both the reference and sample emission spectra were normalized to the 0–1 emission peak at ~580 nm as shown in Fig. S11.

$$\phi_{UC,corr} = \phi_{UC,raw} \times \frac{Int_{Ref}}{Int_{Sample}} \quad \text{S7}$$

Sample (mM)	$\phi_{UC,raw}$ (%)	$\frac{Int_{Ref}}{Int_{Sample}}$	$\phi_{UC,corr}$ (%)
0.095	0.009	1.49	0.013
0.225	0.037	1.80	0.067
0.45	0.082	1.99	0.16
0.849	0.15	2.18	0.32
1.672	0.23	2.30	0.52

Table S1. Table of raw upconversion QY's, correction coefficients and corrected upconversion QY's for TIPS-Tc samples.

Sample (mM)	$\phi_{UC,raw}$ (%)	$\frac{Int_{Ref}}{Int_{Sample}}$	$\phi_{UC,corr}$ (%)
0.039	0.093	1.39	0.13
0.128	0.46	1.76	0.81
0.209	0.86	1.90	1.6
0.392	1.6	2.08	3.3

Table S2. Table of raw upconversion QY's, correction coefficients and corrected upconversion QY's for TIPS-BTX samples.

S12. Kinetic Modeling of TET & TTA Efficiencies

Determining TET efficiency can be done via the results of the Stern-Volmer study and the annihilator triplet lifetime. The excited triplet annihilator concentration $[^3An^*]$ is generated via triplet energy transfer from the triplet sensitizer $[^3S^*]$ with an efficiency dependent on both the ground state annihilator concentration $[An]$ and the natural triplet decay rate constant of the triplet sensitizer $k_{0;T(Sen)}$ shown by Eq. S8.

$$\phi_{TET} = \frac{k_{TET}[An]}{k_{TET}[An] + k_{0;T(Sen)}} \quad \text{S8}$$

Baseline modeling of TTA was done via the simplistic kinetic equation for $[^3An^*]$ shown in Eq. S9 which assumes that the only second order sink for triplet population is TTA from the singlet channel. This is effectively a scenario where the spin statistical factor f discussed in the manuscript is equal to 1, meaning that both the quintet and triplet encounter complex channels do not encounter loss pathways on their own and result only in re-dissociation. A factor of two was included in the TTA decay pathway from the singlet encounter complex channel since two triplets undergo annihilation to form one singlet. The other terms include a source term due to TET and a unimolecular triplet decay term.

$$\frac{d[^3An^*]}{dt} = -2k_{TTA}[^3An^*]^2 - k_{0;T(An)}[^3An^*] + k_{TET}[^3S^*][An] \quad \text{S9}$$

Under this model, the upconversion rate constant k_{TTA} can be determined from the experimentally observed ϕ_{TTA} by Eq. S10. This is the efficiency of TTA relative to other decay pathways for $[^3An^*]$ and is derived from Eq. S9. The factor of $\frac{1}{2}$ is needed in this expression since ϕ_{TTA} (representing the efficiency of triplets annihilating into singlets) is limited to 50 %.

$$\phi_{TTA} = \frac{1}{2} \times \frac{2k_{TTA}[^3An^*]}{2k_{TTA}[^3An^*] + k_{0;T(An)}} \quad \text{S10}$$

The calculation of k_{TTA} requires knowledge of the annihilator triplet decay rate constant $k_{0;T(An)}$ which is measured from the triplet sensitization experiment (see Section S7 above). Given that upconversion experimental measurements were performed under constant excitation, the steady-state approximation can be applied to Eq. S9 for calculating $[^3An^*]$.

$$0 = -2k_{TTA}[^3An^*]^2 - k_{0;T(An)}[^3An^*] + k_{TET}[^3S^*][An] \quad \text{S11}$$

As Eq. S11 is a quadratic expression, $[^3A^*]$ can be solved for as shown in expression S12.

$$[^3An^*] = \frac{k_{0;T(An)} \pm \sqrt{\left(k_{0;T(An)}\right)^2 - 4(-2k_{TTA})(k_{TET}[^3S^*][An])}}{2(-2k_{TTA})} \quad \text{S12}$$

Eq. S12 allows for calculation of $[^3An^*]$ if all parameters are known but is dependent on an additional unknown parameter $[^3S^*]$ (the excited triplet sensitizer concentration). Calculation of $[^3S^*]$ requires an additional kinetic expression referred to as the pumping equation where $[^3S^*]$ derives from the initial laser excitation (Eq. S13)[5]

$$\frac{d[^3S^*]}{dt} = \Phi_{laser}[S_0 - {}^3S^*]\sigma_{sens}\phi_{ISC} - k_{0;T(Sen)}[^3S^*] - k_{TET}[^3S^*][An] \quad \text{S13}$$

1. Φ_{laser} – Photon flux of excitation laser (taken at final measured fluence point). – ~8.6×10^{20} Photons/s*cm^2
2. σ_{sens} – Absorption cross-section of PdPc sensitizer. – 4.01×10^{-16} cm^2 Cross-section determined from measured molar extinction coefficient of ~105,000 M^{-1}cm^{-1} of PdPc at 730 nm.
3. ϕ_{ISC} – Intersystem crossing yield of sensitizer. – 0.75 Value previously discussed in the main text.[2]

The steady-state condition can again be applied to Eq. S11 as shown in Eq. S12.

$$0 = \Phi_{laser}[S_0 - {}^3S^*]\sigma_{sens}\phi_{ISC} - k_{0;T(Sen)}[^3S^*] - k_{TET}[^3S^*][An] \quad \text{S14}$$

Eq. S15 follows from Eq. S14 and allows for the calculation of $[^3S^*]$ based on measurable and reported experimental parameters.

$$[^3S^*] = \frac{\Phi_{laser}[S_0]\sigma_{sens}\phi_{ISC}}{k_{0;T(Sen)} + k_{TET}[An] + \Phi_{laser}\sigma_{sens}\phi_{ISC}} \quad \text{S15}$$

With $[^3S^*]$ in hand, Eqs. S10 and S12 as a system of two equations and two unknowns, the experimentally measured ϕ_{TTA} and relevant experimental parameters of each upconversion sample were used as inputs to solve the system of equations for k_{TTA}. The obtained value was then used to produce the line of best fit for ϕ_{TTA}vs. $[An]$ shown in the main text.

While the results enable adequate modeling of the experimental data as shown in Fig. 5 of the main text, additional excited state decay pathways for $[^3An^*]$ could significantly impact the value determined for k_{TTA}. For example, the net-triplet encounter complex could engage loss pathways rather than just re-dissociation. This could involve an annihilation event (if energetically accessible) producing a ground state annihilator and a higher excited-state triplet that might then decay to T_1. Or in dimers specifically engaging in an encounter complex, internal conversion could take place generating one ground state dimer and one intramolecular ^{3}TT followed by non-radiative decay to T_1 in that excited dimer. In either case, the formation of the net-triplet encounter complex results in the unproductive decay of a single $[^3An^*]$. To be general, Eq. S16 (modification of Eq. S9) can be written with two TTA terms. One describes the productive channel involving the singlet encounter complex which results in a net loss of two $[^3An^*]$. The other illustrates the unproductive channel involving the triplet encounter complex, which is statistically 3x as likely to be formed as the singlet encounter complex, but with a net loss of only a single $[^3An^*]$ apiece. By assuming annihilation from the encounter complex (notwithstanding net-singlet or triplet) occurs at the same rate ($k_{TTA(singlet)} = k_{TTA(triplet)} = k_{TTA}$, Eq. S17), a maximum yield of 20% is implied in Eq. S18. This rate expression is used to describe several upconversion annihilators with accessible higher lying triplet states, such as DPA.[6]

$$\frac{d[^3An^*]}{dt} = -1 \times 2k_{TTA(singlet)}[^3An^*]^2 - 3 \times k_{TTA(triplet)}[^3An^*]^2 - k_{0;T(An)}[^3An^*] + k_{TET}[^3S^*][An] \quad \text{S16}$$

$$\frac{d[^3An^*]}{dt} = -5k_{TTA}[^3An^*]^2 - k_{0;T(An)}[^3An^*] + k_{TET}[^3S^*][An] \quad \text{S17}$$

$$\phi_{TTA} = \frac{1}{2} \times \frac{2k_{TTA}[^3An^*]}{5k_{TTA}[^3An^*] + k_{0;T(An)}} \quad \text{S18}$$

There is an alternative set of kinetics exclusive to dimeric annihilators that we propose may be of interest. The net-quintet encounter complex is assumed to be a decay-neutral complex in monomer systems, due to the lack of an energetically accessible quintet state localized on a monomer. This energetic stipulation likely holds true for dimeric annihilators as well. However, there are now several instances of weakly coupled dimers engaging a ^{5}TT intermediate during dynamics as observed using time-resolved EPR measurements.[7-9] As a weakly coupled dimer itself, TIPS-BTX could in principle harness the net-quintet encounter complex via conversion from the ^{5}TT into the productive ^{1}TT and eventual S_1S_0. In the limit that conversion between the ^{5}TT and ^{3}TT is disallowed, this intramolecular pathway would at best result in an additional gain of the excited singlet state with the loss of two excited triplet states, five times as often as the channel involving solely the net-singlet encounter complex by argument of the spin statistics involved forming the encounter complex (Eq. S19). By once more assuming the rate of annihilation is constant regardless of the initial encounter complex formed, the rate equation simplifies as in Eq. S20. This implies a maximum yield of 40% overall, as is Eq. S21.

$$\frac{d[^3A^*]}{dt} = -1 \times 2k_{TTA(singlet)}[^3An^*]^2 - 3 \times k_{TTA(triplet)}[^3An^*]^2 \quad \text{S19}$$
$$- 5 \times 2k_{TTA(quintet)}[^3An^*]^2 - k_{0;T(An)}[^3An^*] + k_{TET}[^3S^*][An]$$

$$\frac{d[^3A^*]}{dt} = -15k_{TTA}[^3An^*]^2 - k_{0;T(An)}[^3An^*] + k_{TET}[^3S^*][An] \quad \text{S20}$$

$$\phi_{TTA} = \frac{1}{2} \times \frac{12k_{TTA}[^3An^*]}{15k_{TTA}[^3An^*] + k_{0;T(An)}} \quad \text{S21}$$

In the modeling used to determine k_{TTA}, an assumption was made that all second-order decay channels were productive, which when combined with the unimolecular decay channels would give a certain ϕ_{TTA} at a given concentration. If instead other second-order loss channels were made available to the model, the same experimentally measured ϕ_{TTA} at a given concentration would have to be described via a competition between the productive and unproductive second order channels, as well as the inherent unimolecular decay of the triplet state. These additional parameters would increase the calculated k_{TTA} to account for the additional second-order losses. Therefore, the reported k_{TTA} rate constant should be viewed as the lower limit of possibilities.

S13. TD-DFT Results

Table S3. First six singlet excited states for TIPS-Tc

Excited State 1:	Singlet		2.5624 eV	483.86 nm	f = 0.2666	<S**2> = 0.000
72 → 73	HOMO	→	LUMO		0.70426	
Excited State 2:	Singlet		3.6803 eV	336.89 nm	f = 0.0534	<S**2> = 0.000
70 → 73 72 → 75					0.55327 –0.41125	
Excited State 3:	Singlet		3.9419 eV	314.53 nm	f = 0.0401	<S**2> = 0.000
71 → 73 72 → 74					0.65952 –0.21819	
Excited State 4:	Singlet		4.4409 eV	279.19 nm	f = 0.0002	<S**2> = 0.000

71 → 73 72 → 74				0.20542 0.64881	
Excited State 5:	Singlet	4.6456 eV	266.89 nm	f = 2.6646	<S**2> = 0.000
70 → 73 72 → 75				0.41679 0.55573	
Excited State 6:	Singlet	4.7712 eV	259.86 nm	f = 0.0496	<S**2> = 0.000
69 → 73 69 → 74				0.68070 –0.12238	

Table S4. First six singlet excited states for TIPS-BTX

Excited State 1:	Singlet	2.6002 eV	476.82 nm	f = 0.0001	<S**2> = 0.000
204 → 207 205 → 206	HOMO – 1 → HOMO →	LUMO + 1 LUMO		0.49539 0.49873	
Excited State 2:	Singlet	2.6021 eV	476.47 nm	f = 0.5135	<S**2> = 0.000
204 → 206 205 → 207	HOMO – 1 → HOMO →	LUMO LUMO + 1		0.49830 0.49596	
Excited State 3:	Singlet	3.6337 eV	341.20 nm	f = 0.3575	<S**2> = 0.000
198 → 206 200 → 207 203 → 206 204 → 209 205 → 211				0.31148 0.39927 –0.27394 –0.25965 0.26102	
Excited State 4:	Singlet	3.6399 eV	340.63 nm	f = 0.0015	<S**2> = 0.000
198 → 207 200 → 206 203 → 207 204 → 211 205 → 209				0.30839 0.39673 –0.26351 0.27006 –0.26913	
Excited State 5:	Singlet	3.9619 eV	312.94 nm	f = 0.0029	<S**2> = 0.000

199 → 207				–0.28798	
201 → 206				0.46200	
202 → 207				–0.35789	
204 → 210				0.14285	
205 → 208				–0.14234	
Excited State 6:	Singlet	3.9620 eV	312.93 nm	f = 0.0981	<S**2> = 0.000
199 → 206				–0.28954	
201 → 207				0.45900	
202 → 206				–0.36048	
204 → 208				–0.14185	
205 → 210				0.14323	

S14. Molecular Coordinates

Table S5. Ground state geometry coordinates for TIPS-Tc

C	5.08257	-0.71589	0.00003
C	5.08258	0.71585	0.00003
C	3.91181	-1.40793	0.00002
C	2.65248	-0.71958	0.00002
C	2.65249	0.71957	0.00002
C	3.91182	1.40790	0.00002
C	1.44324	-1.39850	-0.00001
C	0.21215	-0.71879	-0.00002
C	0.21215	0.71879	-0.00002
C	1.44325	1.39849	-0.00001
C	-1.02908	-1.41642	-0.00002
C	-2.24532	-0.71903	0.00000
C	-1.02908	1.41643	-0.00002
C	-2.24532	0.71906	0.00000
H	1.44238	-2.48430	-0.00001
H	1.44240	2.48429	-0.00001
H	3.90777	-2.49459	0.00003
H	3.90780	2.49456	0.00003
C	-1.02770	-2.84622	-0.00004
C	-1.02769	2.84623	-0.00004
C	-1.02219	4.05416	-0.00007
C	-1.02231	-4.05415	-0.00007
C	-3.50574	-1.40281	0.00003
C	-3.50573	1.40284	0.00003
C	-4.67813	-0.71371	0.00007
C	-4.67813	0.71374	0.00006
H	-3.50269	-2.48752	0.00003

H	-3.50268	2.48755	0.00003
H	-5.62292	-1.24840	0.00010
H	-5.62291	1.24844	0.00009
H	-1.01911	5.12182	-0.00027
H	-1.01942	-5.12181	-0.00031
H	6.03028	-1.24574	0.00006
H	6.03029	1.24569	0.00006

Table S6. Ground state geometry coordinates for TIPS-BTX

C	4.74932	-0.72314	-0.58490
C	3.30217	-1.14179	-0.72274
C	3.30214	1.14186	-0.72254
C	2.78421	0.00011	-1.63000
H	1.69890	0.00010	-1.75762
H	3.26310	0.00020	-2.61310
C	2.65916	-0.79353	0.64653
C	2.65912	0.79334	0.64667
H	3.13319	-2.16409	-1.06614
H	3.13316	2.16422	-1.06575
C	5.89527	1.42798	-0.45214
C	5.89531	-1.42789	-0.45240
C	7.14573	0.72211	-0.31950
H	5.90363	2.51523	-0.45162
C	7.14575	-0.72201	-0.31963
H	5.90370	-2.51514	-0.45208
C	8.34790	1.39655	-0.19417
C	8.34794	-1.39644	-0.19441
C	9.57571	0.71809	-0.06344
C	9.57573	-0.71797	-0.06357
C	10.80762	1.41566	0.06771
C	10.80766	-1.41553	0.06746
C	12.01910	0.71845	0.19625
C	12.01912	-0.71831	0.19613
C	13.27156	-1.40216	0.32901
C	13.27152	1.40231	0.32924
C	4.74931	0.72322	-0.58476
C	-1.14529	0.69800	0.70863
C	0.00010	1.49299	0.69652
C	-1.14528	-0.69837	0.70855
C	1.14532	0.69818	0.70873
C	-0.00009	2.99551	0.68242
C	0.00018	-1.49329	0.69631
C	-2.65909	0.79323	0.64653
C	1.14533	-0.69841	0.70863

C	0.00003	-2.99581	0.68187
C	-2.65907	-0.79360	0.64655
C	-4.74934	-0.72333	-0.58472
C	-3.30220	-1.14204	-0.72262
C	-4.74929	0.72302	-0.58481
C	-3.30212	1.14160	-0.72271
H	3.15769	-1.28909	1.48367
H	3.15763	1.28878	1.48389
H	-0.02804	-3.39897	1.70122
H	-0.87369	-3.38633	0.15074
H	0.90071	-3.38677	0.19850
H	0.89240	3.38653	0.18406
H	-0.88256	3.38622	0.16619
H	-0.01063	3.39842	1.70221
H	-3.15759	1.28880	1.48369
H	-3.15749	-1.28916	1.48377
C	-2.78428	-0.00027	-1.63008
H	-3.26325	-0.00028	-2.61314
H	-1.69898	-0.00032	-1.75777
H	-3.13339	-2.16441	-1.06587
H	-3.13317	2.16393	-1.06605
C	14.43828	-0.71322	0.45278
C	14.43826	0.71338	0.45290
H	13.26823	2.48709	0.32900
H	13.26830	-2.48694	0.32859
C	10.80640	2.84567	0.06796
C	10.80649	-2.84554	0.06746
C	10.80205	-4.05352	0.06717
C	10.80191	4.05365	0.06779
H	8.34956	2.48244	-0.19508
H	8.34962	-2.48233	-0.19552
C	-5.89533	-1.42805	-0.45208
C	-7.14576	-0.72212	-0.31941
C	-7.14571	0.72200	-0.31953
C	-5.89523	1.42783	-0.45229
C	-8.34795	-1.39651	-0.19408
C	-9.57574	-0.71799	-0.06337
C	-9.57569	0.71807	-0.06352
C	-8.34787	1.39648	-0.19433
C	-10.80768	-1.41551	0.06776
C	-12.01913	-0.71824	0.19625
C	-10.80760	1.41569	0.06746
C	-12.01909	0.71852	0.19609
H	-8.34966	-2.48239	-0.19499
H	-8.34950	2.48237	-0.19545
H	-5.90374	-2.51529	-0.45160

H	-5.90357	2.51507	-0.45196
C	-10.80654	-2.84551	0.06804
C	-10.80636	2.84569	0.06742
C	-10.80185	4.05367	0.06701
C	-10.80212	-4.05349	0.06800
C	-13.27159	-1.40205	0.32922
C	-13.27151	1.40243	0.32891
C	-14.43830	-0.71306	0.45282
C	-14.43826	0.71354	0.45266
H	-13.26834	-2.48683	0.32902
H	-13.26820	2.48721	0.32845
H	15.37760	-1.24830	0.55234
H	15.37757	1.24847	0.55254
H	-15.37764	-1.24811	0.55245
H	-15.37757	1.24866	0.55216
H	10.79987	-5.12113	0.06721
H	10.79979	5.12125	0.06730
H	-10.79972	5.12128	0.06629
H	-10.80002	-5.12110	0.06814

S15. References

1. Gilligan, A. T.; Miller, E. G.; Sammakia, T.; Damrauer, N. H. Using Structurally Well-Defined Norbornyl-Bridged Acene Dimers to Map a Mechanistic Landscape for Correlated Triplet Formation in Singlet Fission. *J. Am. Chem. Soc.* **2019**, *141* (14), 5961−5971.
2. Smyser, K.E.; Eaves, J.D. Singlet fission for quantum information and quantum computing: the parallel *JDE* model. *Sci. Rep.* **2020**, *10* (18480).
3. Murakami, Y.; Kamada, K. Kinetics of photon upconversion by triplet-triplet annihilation: a comprehensive tutorial. *Phys. Chem. Chem. Phys.* **2021**, *23* (34), 18268−18282.
4. Cook, J.D.; Carey, T. J.; Arias, D. H.; Johnson, J. C.; Damrauer, N. H., Solvent-controlled branching of localized versus delocalized singlet exciton states and equilibration with charge transfer in a structurally well-defined tetracene dimer, *J. Phys. Chem. A*, 2017, **121** (48), 9229–9242.
5. Imperiale, C. J.; Green, P. B.; Miller, E. G.; Damrauer, N. H.; Wilson, M. W. B. Triplet-Fusion Upconversion Using a Rigid Tetracene Homodimer. *J. Phys. Chem. Lett* **2019**, *10* (23), 7463–7469.
6. Schmidt, T. W.; Castellano, F. W. Photochemical Upconversion: The Primacy of Kinetics. *J. Phys. Chem. Lett.* **2014**, *5* (22), 4062–4072.
7. Basel, B.; Zirzlmeier, J.; Hetzer, C.; Phelan, B. T.; Krzyaniak, M. D.; Reddy, S. R.; Coto, P. T.; Horwitz, N. E.; Young, R. Y.; White, F. J.; Hampel, F.; Clark, T.; Thoss, M.; Tykwinski, R. R.; Wasielewski, M. R.; Guldi, D. M., Unified model for singlet fission within a non-conjugated covalent pentacene dimer. *Nat Commun* **2017**, *8* (15171).

8. Tayebjee, M. J. Y.; Sanders, S. N.; Kumarasamy, E.; Campos, L. M.; Sfeir, M. Y.; McCamey, D. R., Quintet multiexciton dynamics in singlet fission. *Nature Phys.* **2017**, *13*, 182–188.
9. Dill, R.D.; Smyser, K.E.; Rugg, B.K.; Dmrauer, N. H.; Eaves, J. D. Entangled spin-polarized excitons from singlet fission in a rigid dimer. *Nat. Commun* **2023**, *14* (1180).